Applications in Energy and Combustion Science 12 (2022) 100086

Contents lists available at ScienceDirect

Applications in Energy and Combustion Science

journal homepage: www.elsevier.com/locate/jaecs

Machine learning tabulation of thermochemistry of fuel blends

Tianjie Ding, Stelios Rigopoulos *, W.P. Jones

Imperial College London, South Kensington Campus, London, SW7 2AZ, UK

ARTICLE INFO

Keywords:
Turbulent flames
Machine learning
Artificial neural networks
Chemistry tabulation
Fuel blends

ABSTRACT

The objective of the present work is to develop a machine learning tabulation methodology for thermochemistry that accounts for fuel blends. The approach is based on the hybrid flamelet/random data and multiple multilayer perceptrons (HFRD-MMLP) methodology (Ding et al., 2021), the essence of which is to train a set of artificial neural networks (ANNs) using random data so as to anticipate the composition space encountered in turbulent flame simulations. As such, it is applicable to any combustion modelling approach that involves direct coupling of chemistry and flow, such as transported probability density function (PDF) methods, direct numerical simulation (DNS), conditional moment closure (CMC), unsteady flamelet, multiple mapping closure (MMC), thickened flame model, linear eddy model (LEM), partially stirred reactor (PaSR) as in OpenFOAM and laminar flame computation. In this paper, the HFRD approach is further developed to generate data of varying fuel ratios. Furthermore, radiative heat losses are included and it is shown that the ANN-based simulations are able to account for it. The ANNs generated are first tested on 1-D laminar flame simulations and then applied to two turbulent flames with different fuel compositions: a pure methane flame, Sandia flame D, and Sydney flame HM1, which is a methane/hydrogen flame. The results of species mass fraction and temperature are compared between ANN and direct integration, and excellent agreement are achieved. These results indicate that the methodology has great capacity for generalisation and is applicable to a range of blended fuels. Furthermore, a speed-up ratio of 14 to 17 is attained for the reaction step compared with direct integration, which greatly reduces the computational cost of turbulent combustion simulations.

1. Introduction

In order to attain accurate predictions of emissions in turbulent combustion simulations, detailed multi-species chemical kinetic mechanisms are required. These kinetic mechanisms often involve a large number of reactions and chemical species and a correspondingly large system of differential equations must be solved to determine the evolution of the chemical species. In certain methods, such as the steady flamelet and the Flamelet Generated Manifold (FGM), the chemistry is decoupled from the flow and real-time integration of chemical kinetics is not required. Other methods, however, such as transported probability density function (PDF) methods, direct numerical simulation (DNS), conditional moment closure (CMC), unsteady flamelet, multiple mapping closure (MMC), thickened flame model, linear eddy model (LEM), partially stirred reactor (PaSR) as in OpenFOAM and laminar flame computation, the integration of chemical kinetics must be performed in real time and is usually the bottleneck in the computational performance of such simulations. The direct integration (DI) of the chemical kinetics ODEs, which are often stiff, must be carried out at every grid node and at each time step. If the mechanisms employed involves hundreds of or even thousands of reactions, the DI of the ODEs will take up most of the simulation time, making it computationally intensive or even prohibitive.

One solution for speeding up the computation of chemical kinetics is to employ artificial neural networks (ANN) for chemistry tabulation. ANNs are machine learning models capable of non-linear function approximation and can be trained to approximate the functions determined implicitly by the numerical integration of the chemical kinetics. The resulting CPU gain is due to the fact that the ANNs perform much simpler operations than those involved in the solution of ODEs with implicit methods. Furthermore, no convergence issue is involved, i.e. all composition states are integrated in the same time, while the numerical integration of ODEs can be very slow for composition states that give rise to a stiff system.

Machine learning has recently found many applications in combustion, and a general review can be found in Ihme et al. [1]. The following survey will focus on works related to ANN tabulation of thermochemistry.

In early research including the works of Christo et al. [2–4] and Blasco et al. [5], the ANNs were employed to tabulate simple mechanisms involving only a few species and reactions steps. However, when

* Corresponding author.
E-mail address: s.rigopoulos@imperial.ac.uk (S. Rigopoulos).

https://doi.org/10.1016/j.jaecs.2022.100086
Received 2 June 2022; Received in revised form 12 August 2022; Accepted 27 September 2022
Available online 6 October 2022

it comes to complex mechanisms involving dozens of species, it is difficult to tabulate the chemistry using a single simple ANN, due to the high dimensionality of the composition space. Several methods were developed to solve this problem, including composition partitioning or clustering [6–10], using individual ANNs to predict each reactive scalar [11–13] and using deep neural networks [14,15]. In the work of Ding et al. [16], a method employing multiple multilayer perceptrons (MMLPs) to predict each single species was proposed and shown to substantially improve the ANN prediction accuracy.

The ANNs must first be trained with appropriate data. The generation of the training data is the most challenging problem for ANN chemistry tabulation. If data from the problem to be simulated is employed, agreement can be easily obtained, but the tabulation will not be applicable to other problems. For the ANN tabulation methodology to be of practical use, the data should endow the resulting ANNs with the ability to generalise and be applicable to a range of turbulent combustion problems. Several efforts have been made in this direction. Sen et al. [17,18] generated the training data via stand-alone linear eddy mixing (LEM) simulations. Chatzopoulos et al. [8] proposed a method of training data generation via unsteady laminar flamelet simulations, which was also the basis of the approach in Franke et al. [9]. Wan et al. [14] employed a canonical stochastic micromixing problem to generate the training dataset. An et al. [10] performed a RANS simulation to collect the training data.

In the recent works of Ding et al. [16] and Readshaw et al. [13], a hybrid flamelet/random data (HFRD) sampling method was proposed, where the flamelet sampling of the Chatzopoulos et al. approach was used as a basis for generating a new random dataset. While the flamelet dataset ensured that the starting data were valid and physically meaningful thermochemical states, the random data generation process produced a training dataset that was not limited to the composition regions covered by flamelet solutions and could thus be applied to any combustion modelling approach, including the transported PDF simulations shown in Refs. [13,16]. The ANNs were subsequently applied to the simulation of different methane–air non-premixed flames in the context of the Large Eddy Simulation (LES) — transported probability density function (PDF) approach and excellent agreement with results obtained via direct integration of chemical kinetics was achieved. Notably, in Ref. [16] the Sandia flames D, E and F were all simulated with the same ANNs, thus showing that the HFRD method endows the ANNs with great capacity for generalisation.

Although great progress has been made on ANN chemistry tabulation, so far (to the authors' knowledge) ANNs have only been applied to combustion problems with fixed fuel compositions. However, many works have shown the potential of using blended fuels to improve the efficiency and reduce pollutant emissions of industrial combustion devices. For example, experiments have showed that, by using hydrogen-enriched natural gas, automotive engines can have better performance and reduced emissions at lean conditions [19,20]. As the mixing ratios of the blended fuel varies in different cases, it is impractical to train new ANNs every time a new combustion problem with a different mixing ratios is encountered, especially when one is particularly interested in the influence of fuel mixing ratio. While previous works have shown that the HFRD approach yields ANNs that can generalise to be applied to different flames [13,16], it is desired to develop a set of ANNs applicable to blended fuels with different mixing ratios. Furthermore, in these works the flames were adiabatic, hence one further question pertains to the ability of the ANNs to account for heat losses.

The aim of the present work is to further develop the HFRD method in order to produce ANNs able to account for blended fuels with varying mixing ratios. Furthermore, radiative heat losses are included in order to assess the applicability of the ANNs to non-adiabatic problems. The MMLP method [16] is also applied in order to improve the ANN prediction accuracy. Methane flames with hydrogen enrichment are chosen as the target flames and the complete GRI-1.2 mechanism [21] is employed for ANN tabulation.

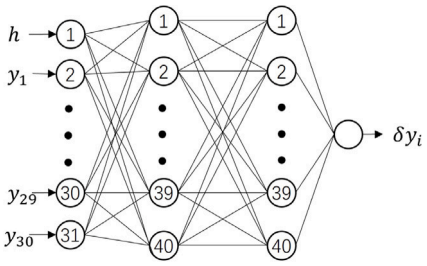

Fig. 1. MLP structure.

The paper is structured as follows. Section 2 describes the methodology, with emphasis on the new elements in the present paper. Section 3 evaluates the performance of the ANNs on one-dimensional problems, while in Section 4 the target turbulent flames are simulated and discussed, followed by the conclusions.

2. Machine learning tabulation methodology

2.1. Overview

For a given chemistry mechanism, the species concentrations after a simulation time step δt can be calculated given their initial states by numerically integrating the ODEs that describe the time evolution of the reaction system. For reactions under a fixed pressure, the initial states can be fully described by the species concentrations y_i and the specific enthalpy h, and the species concentration change δy_i during the reaction time step δt can be expressed as a function of y_i and h:

$$\delta y_i = F(y_i, h) \tag{1}$$

where F is a function that is implicitly determined by the solution of the chemical kinetics ODEs. Note that the specific enthalpy includes the enthalpy of formation and does not change due to chemical reaction.

ANNs have the ability to approximate highly nonlinear functions. Therefore, the function F can be represented by ANNs so that the time-consuming direct integration of chemical kinetics can be replaced by ANN chemistry tabulation. The ANN model employed in this work is the multilayer perceptron (MLP), a widely used model for nonlinear function fitting. An MLP consists of several layers of neurons and a schematic of the MLP employed in this work for predicting a single species is shown in Fig. 1, using two hidden layers containing 40 neurons each. The target chemistry mechanism to tabulate in this work is the GRI-1.2 mechanism, involving 31 species (if Ar is not considered). The concentration of N_2 does not change during the reaction and its influence on other species is negligible, so N_2 is not used as an input to MLP. Therefore, the MLP has a total of 31 inputs (30 species + enthalpy). The hyperbolic tangent function is used as the activation function of the hidden layers, while a linear function is used for output layer. All MLPs use the same structure, which is shown in Fig. 1.

The ANNs must first be trained with a training dataset. During the training process, the parameters of the ANNs are adjusted to fit a set of input and output data. In the present work, all ANNs are trained using the MATLAB neural network toolbox and the training algorithm employed is Bayesian Regularisation. The MLP structure and training algorithm settings are the same as those in our previous work [16].

The most important aspect of the methodology is the generation of training data, as the objective is to generate them in an abstract manner that anticipates the composition space encountered in turbulent flame simulations. For this reason, in our previous works [13,16] we proposed an approach where the data were generated via a random procedure, using data from laminar flamelets as a starting point. The

role of the flamelet data was to provide a robust basis for creating data with valid compositions, but they were subsequently discarded and only the random data were employed, as they cover a much wider composition space and have a generalisation capacity that is not limited by the states encountered in flamelet simulations. Nevertheless, the data were still limited by the fuel composition of the initial flamelet data. In the present work, this approach is augmented to generate data suitable for a much wider range of flames that feature variable fuel ratios.

2.2. A random data generation method for fuel blends

The basics of our hybrid flamelet/random data (HFRD) generation approach will be described here succinctly, and only the new developments will be described in detail. More basic details of HFRD method can be found in Refs. [13,16].

The training data are generated in two steps: sampling via flamelet simulations and random data generation. For the first step, 1-D laminar counterflow diffusion flamelet simulations are performed to collect data samples. This canonical combustion problem is governed by the following equation [22]:

$$\rho\frac{\partial y_i}{\partial t} = \rho\frac{\chi(z)}{2}\frac{\partial^2 y_i}{\partial z^2} + \dot{\omega}_i \tag{2}$$

Here z is the mixture fraction, y_i is the species concentration, $\dot{\omega}_i$ is the reaction rate and χ is the scalar dissipation rate given by the following equation:

$$\chi(z) = \frac{S}{\pi}\exp\left[-2(\mathrm{erfc}^{-1}(2z))^2\right] \tag{3}$$

where S is the strain rate.

Following our previous works [13,16], the initial fuel and oxidant temperatures use random values for each flamelet simulation. However, these works were targeting methane flames only. In order to collect samples corresponding to methane flame with different levels of hydrogen enriched, the fuel of the flamelet simulation in this work is set as a mixture of CH_4 and H_2, and the molar ratio of H_2/CH_4 is randomly chosen between 0 and 2 for each flamelet simulation. The strain rate is also randomly chosen between 1/s and a value higher than the extinction strain rate. Flamelet simulations using very low strain rates will produce samples close to equilibrium states, while flamelets with very high strain rates can produce samples representing extinction states. In our previous works [13,16], the maximum strain rate is set to a fixed value. However, in the case of methane/hydrogen blended fuels, the extinction strain rate is highly influenced by fuel mixing ratio. With increasing H_2/CH_4 ratio from 0 to 2, the extinction strain will also increase from about 600/s to 2000/s. Therefore, the maximum strain rate should be set as a function of mixing ratio. In this work, the following equation is used for determine the maximum strain rate:

$$S_{max} = 800 + 800m \tag{4}$$

where m is the H_2/CH_4 ratio. There is no need to know the precise values of extinction strain rate for different mixing ratios. The only requirement is that the S_{max} is reasonably higher than the extinction strain rate, hence a simple linear equation is sufficient for choosing the maximum strain rate.

Table 1 lists the minimum and maximum values for several flamelet simulation parameters. In this work, a total of 200 flamelet simulations are performed, with different random strain rates, initial temperatures and H_2/CH_4 molar ratios. The data are collected within the mixture fraction flammability range, which is defined as the total element mass fraction of C and H in this work. Although the upper and lower flammability limits of CH_4 vary if different concentrations of H_2 are introduced, the mixture fraction range employed in this work is (0.01,0.14) and is wide enough to cover the actual flammability range for CH_4/H_2 fuel if the fuel molar ratio of H_2/CH_4 is not larger than 2.

Table 1
Initial conditions of flamelet simulations.

Variables	Minimum	Maximum
Initial temperature of fuel (T_f)	150 K	350 K
Initial temperature of oxidant (T_o)	150 K	350 K
H_2/CH_4 fuel mixing ratio (m)	0	2
Strain rate (S)	1/s	800 + 800 m

Table 2
Constraints for random data generation.

Variables	Minimum	Maximum
H/C ratio	3.9	8.1
O/N ratio	0.26	0.27
Temperature	500 K	–
Mixture fraction	0.01	0.14

After the flamelet simulations, the flamelet dataset is used as a basis to generate the random dataset. For each data state (h and y_j) of the flamelet dataset, a new random state can be generated using the following equations:

$$h_{rnd} = h + \frac{c}{a}(h_{max} - h_{min}) \tag{5}$$

$$y'_j = y_j^{(1+c/b)} \quad (j \neq j_{N2}) \tag{6}$$

$$y'_{N_2} = y_{N_2} + \frac{c}{a}(y_{N_2,max} - y_{N_2,min}) \tag{7}$$

$$y_{j,rnd} = \frac{y'_j}{\sum y'} \tag{8}$$

The new enthalpy value h_{rnd} is generated based on the origin enthalpy h, the minimum enthalpy h_{min} and the maximum enthalpy h_{max} of the flamelet dataset. It should be noted that, by allowing enthalpy to take values from a range, the approach allows the resulting ANNs to be applicable to cases with heat losses, and this feature will be discussed further in Section 2.3. For all species except N_2, the new species concentration value y'_j is generated based on its initial value y_j. The variable c is a random value uniformly distributed in the range (−1,1). The choice of parameters a and b will be discussed later in the present section. The concentration of N_2 does not change during the reaction and has similar order of magnitude for all flamelet states. Therefore, Eq. (7) is used to generate the random N_2 concentration, and has the same form as the equation for random enthalpy generation. After a new random state is generated, Eq. (8) is introduced to normalise the species concentrations, in order to ensure that the species mass fractions sum to unity.

In additional to mass conservation, the new random state should also satisfy element ratio constraints. Assuming equal Schmidt numbers, the fuel ratio of H_2/CH_4 is between 0 and 2, hence the element molar ratio of H/C is between 4 and 8. The oxidant is air, hence the element molar ratio of O/N should be the same as that of air. In order to make the random data more generalised, the element ratio constraints are relaxed to reasonable ranges. In this work, the H/C and O/N ratio range for random data is set to (3.9,8.1) and (0.26,0.27) respectively. The states with temperature below 500 K or mixture fraction outside of the range (0.01,0.14) will also not be considered due to their low reactivity. All the constraints that the random data must satisfy are shown in Table 2. However, there is no guarantee that the generated random state will automatically satisfy all these constraints. Therefore, for each flamelet state, the random state is generated using Eqs. (5) to (8) repeatedly until all constraints in Table 2 are satisfied, or the flamelet state is abandoned after 100 unsuccessful iterations.

To generate appropriate random dataset, the values of a and b in Eqs. (5) and (6) should be chosen properly. Small values of b will make the random state difficult to satisfy all of the constraints in Table 2 and also generate states too far from the initial flamelet-sampled states,

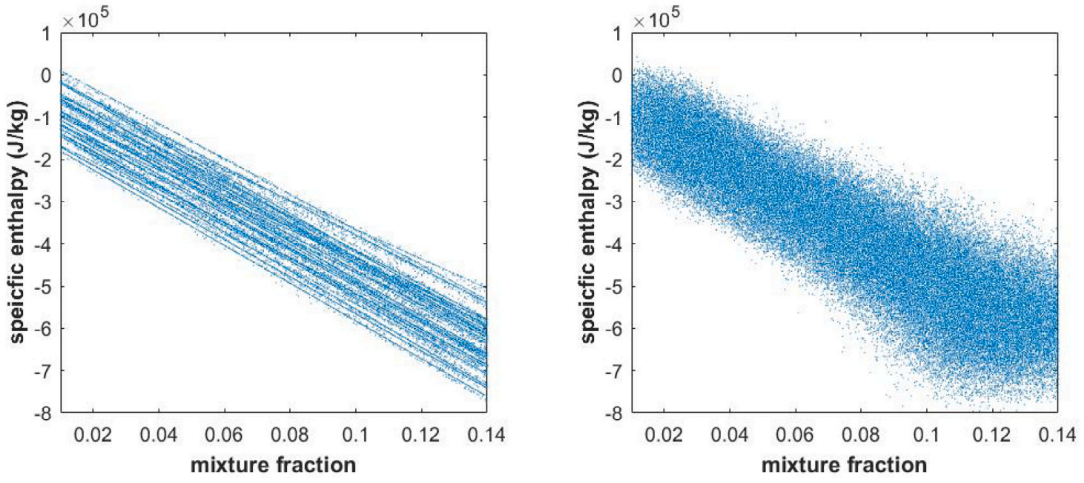

(a) Flamelet dataset (b) Random dataset

Fig. 2. Mixture fraction versus enthalpy comparison between flamelet dataset and random dataset.

which are likely to be non-physical. On the other hand, large values will lead to states too close to the flamelet-sampled ones, thus making the random data less capable for generalisation. A simple way to check whether the random data is appropriate is to compare it with the flamelet dataset. Scatter plots of major species, mixture fraction or enthalpy can be drawn. An ideal random dataset should eliminate all patterns caused by the flamelet sampling procedure and cover a similar or a slightly wider composition space, as compared with the flamelet dataset. In the present work, the values of a and b are set to 10, and the specific enthalpies in both the flamelet and the random dataset are plotted against mixture fraction values in Fig. 2. It can be seen that, in Fig. 2(a), the flamelet samples are concentrated along several lines, except for data with numerical errors. Overall, compared with the flamelet dataset, the random dataset is more general and covers better the composition space of the blended CH_4/H_2 flames. It should also be emphasised that the flamelet data is used merely as guidance for generating new composition states via the random process and are then discarded. The role of the flamelets is merely for generating valid composition states to be used as starting points; neither the states nor the diffusion–reaction structure of the flamelets are employed in the method.

The fuel mixing ratio and initial temperatures are randomly set for the flamelet simulations. Once set, a linear relationship between enthalpy and mixture fraction is determined and therefore the samples collected from a specific flamelet simulation are located on the same line in the 2-D mixture fraction-enthalpy space. The whole flamelet dataset runs along several such lines, with each line corresponding to a individual flamelet simulation. The linear relationship between enthalpy and mixture fraction will significantly influence the generalisation capacity of the resulting ANNs. Directly applying the flamelet dataset to training is likely to cause biased ANNs, especially when heat losses are considered, where the enthalpy and mixture fraction are not linearly related. By applying the random data generation method, the linear relations caused by the flamelet sampling method can be eliminated, as shown in Fig. 2(b). Therefore, the ANNs trained using the random data can have much greater capacity for generalisation compared with those trained with the flamelet dataset. The enthalpy range of the random data is also slightly further expanded, making the data more suitable for combustion problems with heat loss. The overall composition space covered by the random dataset is quite similar to that of the flamelet dataset, which means that the values chosen for the coefficients a and b in Eqs. (5) and (6) are appropriate.

In the present work, a total of about 1,000,000 flamelet samples are collected and about 950,000 random data are generated. The random state will then undergo a single reaction step using direct integration, and the resulting concentration change will be used as the target output for ANN training. The time step employed in this work is 10^{-6} s and the direct integration was performed with the VODE solver [23]. Note that, if dynamic time stepping is desired, the ANNs trained for a minimum fixed time step can be called in succession; it is also possible to train more than one set of ANNs with different time steps and use combinations of them. The same solver and time step were also employed for the laminar flame simulations and turbulent combustion simulations that will be shown in the following sections.

2.3. Non-adiabatic flames

Due to the wide range of initial temperature employed for the flamelet simulations, the dataset collected will have a wide range of enthalpies, hence the states encountered in non-adiabatic flames can be properly covered. This is shown in Fig. 3, using data from the simulation of Sandia flame D that will be described in Section 4.1. The simulation includes radiative heat loss and the enthalpy of the sampled Sandia D thermochemical states is plotted against the mixture fraction. The lines shown represent the methane/air mixtures at different temperatures. These lines also correspond to flamelet simulations with different initial temperatures, as the relationship between enthalpy and mixture fraction will not change during the flamelet simulation if no heat loss is considered. It can be seen that most of the Sandia flame states are located between the yellow and orange lines. Therefore, to cover the composition space of Sandia flame D, the initial temperature of the methane flamelet simulation should cover the range from 200 K to 300 K. If the flamelet simulations are only performed with room temperature or with a small initial temperature range, the states with low enthalpy will not be covered, hence the dataset collected will not be suitable for non-adiabatic problems. For methane flames with hydrogen enrichment, the slope of the enthalpy-mixture fraction line will slightly changed, but the enthalpy range covered are still similar, as can be seen in Fig. 2(a). Therefore, for methane/hydrogen blended fuels, it is still necessary to employ a wide range of initial temperature for the flamelet simulations. The temperature range employed in this work is from 150 K to 350 K, completely covering the composition states of Sandia flame D, as well as many other non-adiabatic turbulent flames.

2.4. Multiple MLPs method

In the present work, the Multiple multilayer perceptrons (MMLP) approach proposed in our previous work [16] is applied. This method

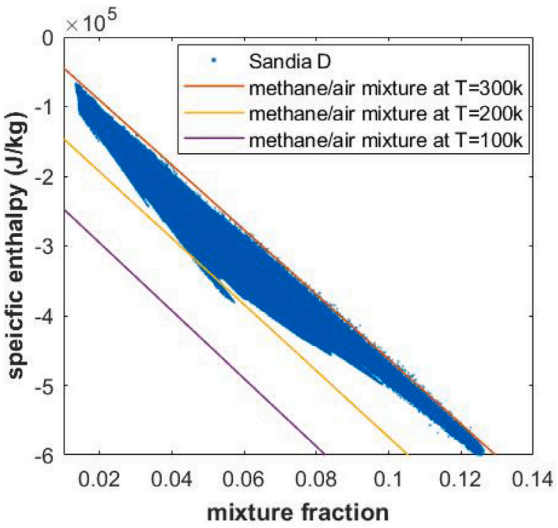

Fig. 3. Enthalpy versus mixture fraction for a methane/air mixture at different temperatures and for the Sandia D flame. (For interpretation of the references to colour in this figure legend, the reader is referred to the web version of this article.)

can greatly improve the ANN prediction accuracy, especially for the species with small concentration changes during reaction. The main idea of the MMLP approach is briefly described here, while one may refer to our previous work [16] for more details.

Most of the ANN training algorithms aim to minimise the sum of squares errors between ANN predictions and target outputs. When applying the entire random dataset for MLP training, the MLP outputs will have similar absolute errors, regardless of their target output value. Even if the absolute errors are very small, the relative errors can still be very large for outputs with small values, especially when the outputs are of the same of even smaller magnitude as the absolute errors. For example, if the output range of a target species is $(-k, k)$, the MLP error may be of the order of $k/100$. For large output values of order k, both the relative and absolute error are small. However, if the output value is within the range $(-k/10, k/10)$, then the relative error is about 10%. In our previous work [16], it was found to be difficult for an MLP to achieve both low absolute errors for data with large output magnitudes and low relative errors for data with small output magnitudes, as these data usually correspond to states with different dynamical behaviour.

The MMLP method can be employed to improve the prediction accuracy for data with small output magnitudes. For example, for data with output range $(-k/10, k/10)$, a separate MLP can be trained using the random data whose outputs are within the given range. The new MLP will only learn from the data within the corresponding range, so its performance on these data will be greatly improved as compared with the MLP trained using the entire random dataset. However, even for the new MLP, the prediction errors may still be large for data with smaller output values (e.g. data with output range $(-k/100, k/100)$). The prediction accuracy of such data can be further improved by training another new MLP focussing only on these data. However, it is found that the improvement on prediction accuracy reduces with each new iteration. Therefore, when a new MLP with a smaller output range is trained, it is tested and accepted only if its performance on the data with this target output range is improved. Finally, for each species, multiple MLPs are trained, with each predicting states with different magnitudes of species concentration changes.

The root mean square errors (RMSE) of multiple MLPs for several major species, tested on flamelet dataset, are shown in Fig. 4. In the case of CH_4, the prediction error of the target outputs within the range $(-10^{-5}, 10^{-5})$ is reduced by about 50% by the second MLP (orange bar), while the third MLP (yellow bar) further improves the prediction accuracy for outputs within range $(-2 \times 10^{-6}, 2 \times 10^{-6})$. Similarly, the prediction error for O_2 is reduced when applying multiple MLPs. However, in the case of CO and H_2, only the second MLP reduces the prediction error while the third MLP fails to further improve accuracy, which means that 2 MLPs are enough and there is no need to introducing new MLPs for H_2 and CO.

When applying the multiple MLPs, the input data will start with the last MLP which has the narrowest output range. If its prediction falls within the corresponding output range, then the prediction will be accepted. Otherwise, the data will go to previous MLP with a wider output range, and the above process will be repeated until the data goes to the first MLP with the widest output range, in which case the prediction of the first MLP will be the final output.

In the present work, 2 to 3 MLPs are trained for each species, resulting a total of 71 MLPs. Each ANN is trained for 1500 epochs using 100,000 training data, and the training time for a single MLP is about 20 h using a single Xeon 6132 2.6 GHz core. All the ANN training can be carried out on a workstation with about 30 to 40 cores in parallel and takes a couple of days in such a configuration. The training time is negligible when compared with the simulation time needed for direct integration — for the flames in the present work, hundreds of cores must be employed for several weeks. Furthermore, the ANNs can be trained once and used for several different turbulent flames, as will be demonstrated later. The storage required for storing the MLP parameters is also extremely small (about 5.5 MB in this case).

3. Application to one-dimensional laminar flames

Before applying the ANNs to turbulent combustion simulations, they will first be tested on 1-D laminar flamelets and 1-D laminar premixed flames, with both pure and blended fuels. For the laminar flamelet simulation, the mixture fraction space is discretised with 200 nodes and grid refinement around the stoichiometric mixture fraction. For 1-D premixed flames, the simulation domain is set to 0.01 m and employs 200 nodes with refinement around the flame front. Differential diffusion is also employed for the premixed flames, thus putting to test the ability of the HFRD method to deal with variable element ratios. For each individual flame, the simulations are carried out with both ANNs and direct integration, and their results are compared to evaluate the performance of the ANNs.

3.1. Methane flames

The ANN chemistry tabulation method in the present work is developed for blended methane/hydrogen fuels with H_2/CH_4 ratio varying from 0 to 2, which means that the ANNs should also work on pure methane–air flames. Therefore, before the application to blended fuels, it is important to ensure that no significant loss of accuracy is incurred when the method is applied to pure methane flames, due to the extension to blended fuels. Therefore, it is necessary to test the ANNs on pure methane–air flames first and compare the results with those obtained in our previous works [16], where the ANNs were trained for methane flames only.

A flamelet simulation with strain rate equal to 100/s and initial temperature of 300 K, and a 1-D premixed flame with an equivalence ratio of 1 and an initial temperature of 300 K are employed to evaluate the performance of the ANNs on methane–air flames. The simulation results for the laminar flamelet are shown in Fig. 5, where the species mass fraction and temperature (T) profiles around the mixture fraction flammability range ($0 < z < 0.15$) are plotted. The results for the 1-D laminar premixed flame are shown in Fig. 6, with the species mass fractions and temperature (T) shown along the simulation domain ($0 < x < 10$ mm). In both cases, it can be clearly seen that the ANN results are in very good agreement with the DI results. The ANN and DI profiles are virtually coincident and the errors are too small to be distinguishable.

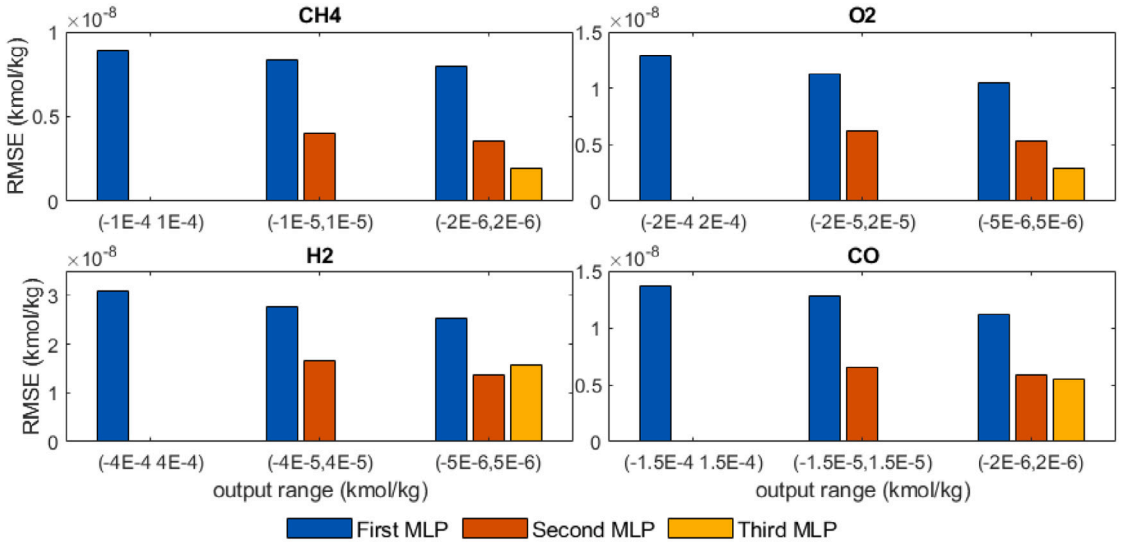

Fig. 4. RMSE comparison of multiple MLPs for several major species. (For interpretation of the references to colour in this figure legend, the reader is referred to the web version of this article.)

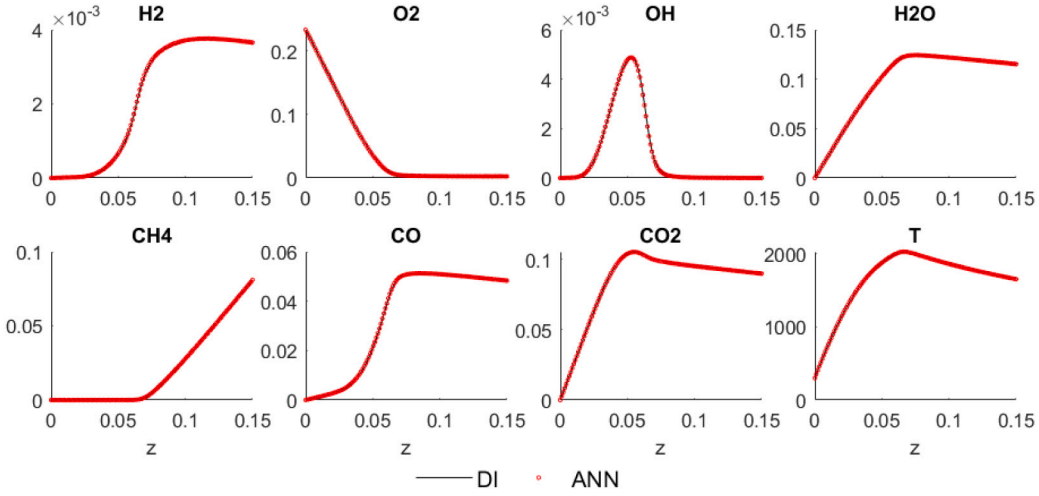

Fig. 5. Species mass fractions and temperature profiles in the methane–air flamelet simulation. The DI results are plotted in black solid lines, while the ANN results are shown using red circle symbols. (For interpretation of the references to colour in this figure legend, the reader is referred to the web version of this article.)

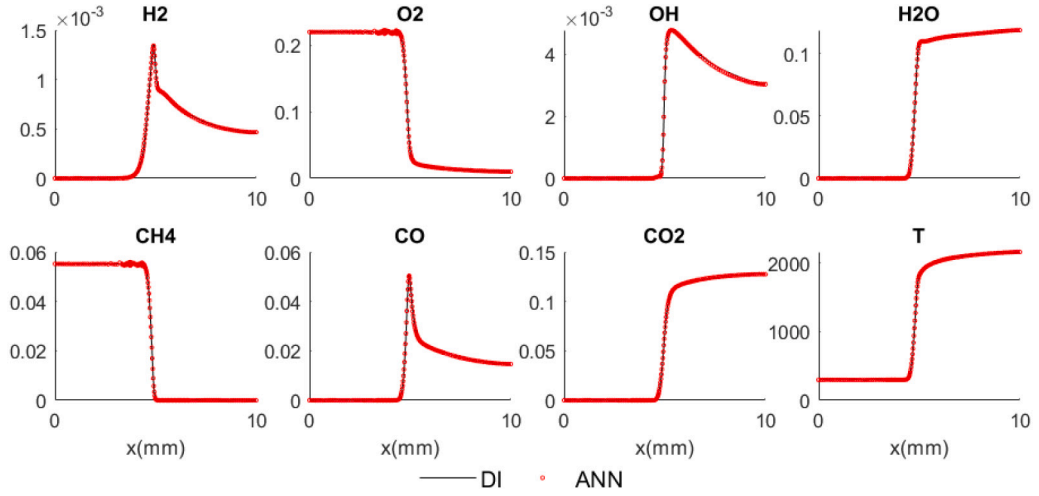

Fig. 6. Species mass fractions and temperature profiles in the 1-D premixed methane flame simulation. The DI results are plotted in black solid lines, while the ANN results are shown using red circle symbols. (For interpretation of the references to colour in this figure legend, the reader is referred to the web version of this article.)

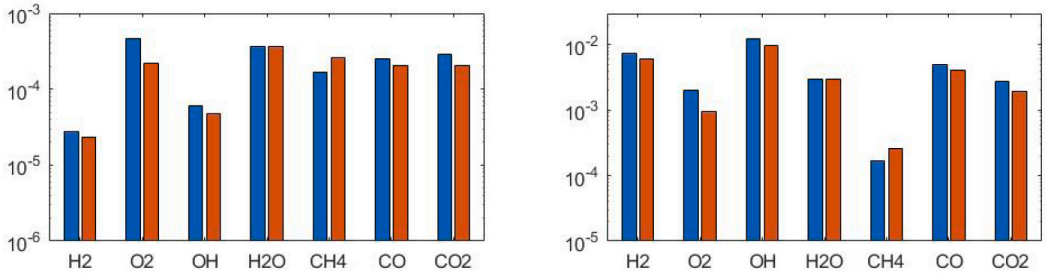

(a) Absolute error (b) Relative error

Fig. 7. Error comparison of the laminar flamelet simulation results using different ANNs. The blue bars show the ANN errors in the present work, while the red bars represent the ANN errors in Ref. [16] where the ANNs were trained for pure methane flames. (For interpretation of the references to colour in this figure legend, the reader is referred to the web version of this article.)

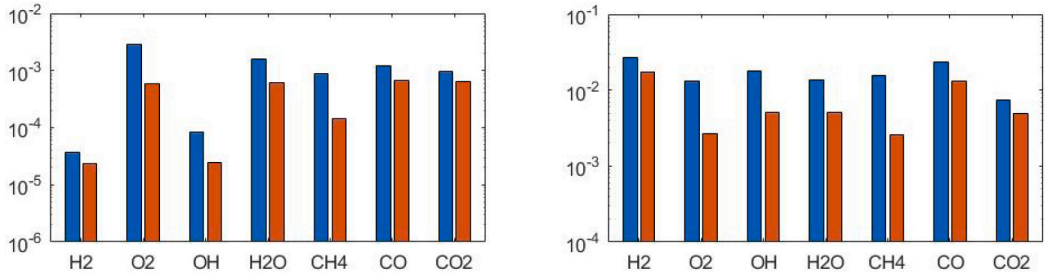

(a) Absolute error (b) Relative error

Fig. 8. Error comparison of the 1-D premixed flame simulation results using different ANNs. The blue bars show the ANN errors in the present work, while the red bars represent the ANN errors in Ref. [16] where the ANNs were trained for pure methane flames. (For interpretation of the references to colour in this figure legend, the reader is referred to the web version of this article.)

To quantitatively analyse the ANN performance, the maximum absolute errors between ANN results and DI results for the target species i are calculated using the following equation:

$$\text{absolute error} = \max\left[\text{abs}(n_i^{ANN} - n_i^{DI})\right] \tag{9}$$

where n_i^{ANN} and n_i^{DI} are the simulation results (species mass fraction or temperature) of ANN and DI respectively. The absolute errors are also normalised by the maximum value obtained via DI in order to calculate the relative error:

$$\text{relative error} = \frac{\max\left[\text{abs}(n_i^{ANN} - n_i^{DI})\right]}{\max(n_i^{DI})} \tag{10}$$

For comparison, the ANN errors in our previous work [16], which targeted methane flames only, are also calculated. The errors are shown in Figs. 7 and 8, and both absolute errors and relative errors are calculated. In the case of the flamelet simulation, it can be seen that the errors in both works have a similar order of magnitude. The maximum relative error is only about 1%, which occurs on OH. In the case of the premixed flame, the ANN error for the blended fuel ANNs is 1.5 to 5 times higher than that of the ANNs trained for pure methane. Despite this increase, the overall errors are still very small compared with the mass fraction of the species and are hardly distinguishable. The maximum relative error shown in Fig. 8b is only about 3%, which occurs on H_2. It can thus be concluded that the ANNs developed for blended fuels still perform very well on pure methane flames.

3.2. Blended methane/hydrogen flames

After the test on pure methane flames, the ANNs are now tested on methane/hydrogen flames, which is the main focus of the present work. In order to extent the enthalpy range, low-temperature flames are also used for testing. Strain rate (in the case of laminar flamelets) and equivalence ratio (in the case of laminar premixed flames) are also set to different values for different cases, in order to better demonstrate the generalisation capacity of the ANNs.

Three flamelet simulations and three 1-D laminar premixed flames are first performed, with their parameters listed in Tables 3 and 4 respectively. For each case of the same type of flame, all three flame parameters are set to be different from other two cases. Case 1 and Case A feature low level hydrogen enrichment, while Case 3 and Case C feature high level of hydrogen enrichment. Case 1 features low strain rate while case 3 features high strain rate. Case A uses high initial temperature while Case 2, 3 and C uses low initial temperature. The simulation results of laminar flamelet cases are shown in Fig. 9, where the profiles of temperature, several major species and several minor species are plotted over mixture fraction around flammability range. It can be clearly seen that the ANN results are in excellent agreement with the DI results in all three cases and even the minor species can be accurately predicted by the ANNs. The simulation results of three 1-D premixed laminar flames are shown in Fig. 10. Most species and temperature are plotted over the whole domain ($0 < x < 10$ mm) while some minor species are plotted around the flame front (4 mm $< x <$ 6 mm) in order to clearly show the profile. Overall, excellent ANN prediction accuracy is obtained in all 3 cases. In case A, the ANN and DI profiles virtually coincide for all species and temperature. In case B, only C_2H_6 is slightly underpredicted. The ANN predictions of other species are highly accurate. In case C, the ANN results of H, O and OH are slightly underpredicted in the fully burnt side, but the errors are small and overall the profiles are in good agreement with those obtained via DI. The simulated flame speeds for the premixed flames are listed in Table 5, and very good agreement is achieved between ANN and DI. The relative error of the ANN prediction is also calculated and its maximum is 2.3%, which occurs in case C.

It is worth noting that, while the laminar flamelet is the problem used to collect the initial data that was used for the random data generation, the 1-D laminar premixed flame is a different problem and

Table 3
Flamelet test cases.

Case	H_2/CH_4 ratio	Initial temperature	Strain rate
1	0.5	300 K	50/s
2	1.0	275 K	500/s
3	2.0	250 K	1500/s

Table 4
1-D premixed flame test cases.

Case	H_2/CH_4 ratio	Initial temperature	Equivalence ratio
A	0.2	320 K	0.8
B	1.0	300 K	1.0
C	1.8	280 K	1.2

Table 5
Flame speed of 1-D premixed flames as calculated by ANN and DI simulations.

Flame case	Flame speed simulated via DI (m/s)	Flame speed simulated via ANN (m/s)	Relative error
A	0.3557	0.3631	2.08%
B	0.6380	0.6361	0.30%
C	0.7732	0.7554	2.30%

no data from it was involved in the training data generation. This may explain the minor discrepancies found in the premixed flame, but the accuracy there is still remarkably high and indicates that the ANNs have a good capacity for generalisation.

4. Applications to turbulent flames

In order to validate the ANN methodology, two turbulent flames with different fuel compositions were chosen as test cases in this work. The first case is the Sandia piloted jet flame D, the fuel of which is methane and air. The second test case is the Sydney bluff body flame HM1, which is a methane/hydrogen flame. These two flames are well studied and the detailed experiment data are available on the "International Workshop on Measurement and Computation of Turbulent Nonpremixed Flames" (TNF Workshop) [24]. The Sandia flame was also simulated successfully in our previous work [16], where the methodology targeted methane flames only. Although the ANNs are successfully applied to 1-D laminar methane flames, their performance on turbulent methane flames is still unknown. It is therefore necessary to simulate the Sandia flame D again with the extended methodology in order to ascertain that no loss of accuracy is incurred by the varying fuel ratio data. Afterwards, the simulation of the Sydney HM1 flame is performed, which has a more complicated flame structure than the Sandia flames, in order to put the new features of the approach to test.

In the present work, the turbulent flames are simulated with the LES stochastic field method, the implementation of which is almost identical to that described in the work of Jones et al. [25], with the addition of radiative heat loss. The simulations employed eight stochastic fields and the dynamic Smagorinsky model of Piomelli and Liu [26]. Equal diffusivities were also assumed, with a Schmidt number of $\sigma_{sgs} = 0.7$. The simulations were performed with our in-house CFD code BOFFIN [27]. A semi-implicit scheme was employed for temporal discretisation, while the central difference scheme was employed for spatial discretisation, except for the convective terms of the scalar equations, which were discretised using a total variation diminishing (TVD) scheme. More numeric details about the BOFFIN code can be found in Ref. [25] and the thesis of Prasad [28]. The radiative heat loss is considered in our simulations using the optically thin radiation model, with radiative properties based on the RADCAL model [29]. CH_4, CO, CO_2 and H_2O are considered for radiation and the detailed description of the model is documented in Ref. [30]. For each flame, two simulations were carried out, one using DI and another one using the ANNs for the reaction source term computations. Once the flame had become fully developed, the statistical quantities (mean and RMS) were collected for a period of more than 5 flowthrough times (based on bulk velocity of the jet). After that, the collected statistics were compared between DI and ANN.

Table 6
Average CPU time for the Sandia flame D simulation.

Method	Reaction time (t_R)	Total time (t_T)	t_R/t_T
DI	1	1.27	78%
ANN	0.057	0.41	14%

4.1. Sandia flame D

The Sandia flames are piloted partially premixed jet flames, studied experimentally by Barlow et al. [31] and Schneider et al. [32]. This flame series, especially flame D, has been widely used to validate combustion models. The burner of Sandia flames has a main jet diameter (D) of 7.2 mm and a pilot diameter of 18.2 mm. The jet composition is 25% CH_4 and 75% air by volume. The annular pilot burnt composition has the same specific enthalpy and equilibrium composition as a CH_4/air mixture at equivalence ratio $\phi = 0.77$. For flame D, the bulk velocities of the jet, pilot and coflow are 49.6 m/s, 11.4 m/s and 0.9 m/s respectively. The simulation domain has dimensions 36 (axial) × 7.5 × 7.5 cm and a Cartesian grid with three million cells is employed. The grid cells are evenly distributed in the downstream direction. In the radial direction, the cell size is about 0.5 mm in the central jet region and then expands smoothly towards the outside boundary. Using a time step of 10^{-6} s, the maximum CFL number is less than 0.1.

Figs. 11 and 12 show the radial profiles of species mass fraction and temperature at 4 axial locations: Z = 7.5D, 15D, 30D and 45D. The DI results and ANN results are compared, while the experimental data are also shown. It can be seen that the ANN results are in excellent agreement with the DI results. For most major species and temperature in Fig. 11, the ANN profiles and DI profiles are highly coincident for both mean value and RMS value, and the differences are too small to be distinguishable in the figure. For minor species shown in Fig. 12, the ANN profiles and DI profiles are almost identical at location Z = 7.5D and 15D, while small discrepancies can be found near the centreline at location Z = 30D and 45D. However, the errors are very small and the overall ANN results are still in very good agreement with DI results.

The mean temperature field and CH_4 mass fraction contours are plotted in Fig. 13. Both ANN results and DI results are shown for comparison. It can be seen that the distribution of these two scalar fields between ANN and DI are highly consistent, which means that the ANNs can reproduce the flame structure with high accuracy.

The CPU time comparison of the Sandia flame D simulation using ANNs and DI is shown in Table 6, taken after the flame has been fully developed (note that the time is normalised with the reaction time using DI). Great savings in computational cost are achieved using ANNs, with the CPU time taken for the reaction step reduced by 94% corresponding to a speed-up ratio of 17.5% (see Table 6).

4.2. Sydney HM1 flame

The burner of the Sydney bluff body flame consists of a fuel jet of diameter 3.6 mm, surrounded by a solid cylindrical bluff body of diameter 50 mm. The fuel consists of 50% methane and 50% hydrogen (volume percentage). The experimental study of a series of Sydney bluff body flames, with different inflow velocities, were conducted by Dally et al. [33]. In the present work, the HM1 flame is used to validate the ANN thermochemistry tabulation methodology. The bulk velocities of the jet and coflow air are 118 m/s and 40 m/s respectively. The simulation domain has cylindrical dimensions 25 (axial) × 7.5 (radial) cm, resolved by and a grid with about two million cells. The grid is

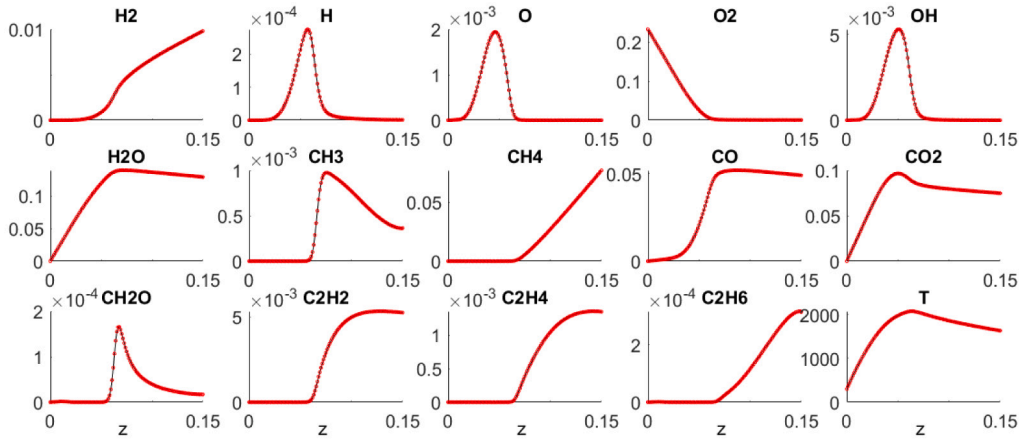

(a) Case 1.

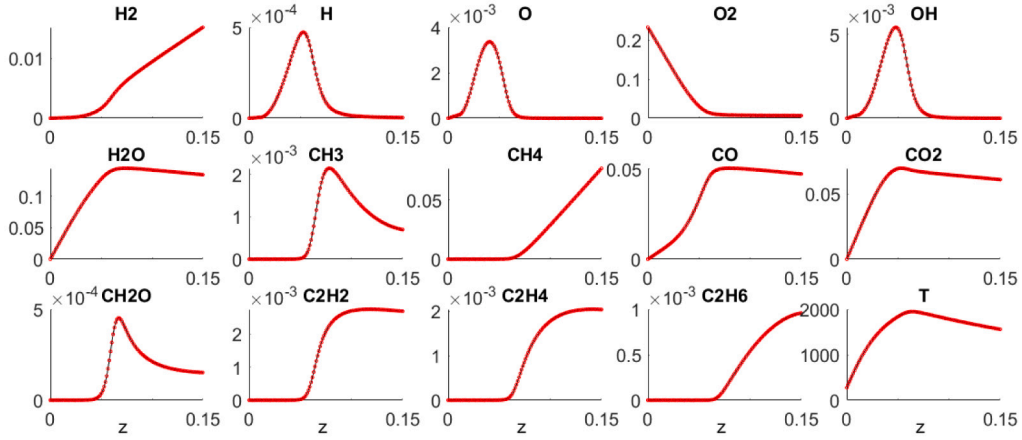

(b) Case 2.

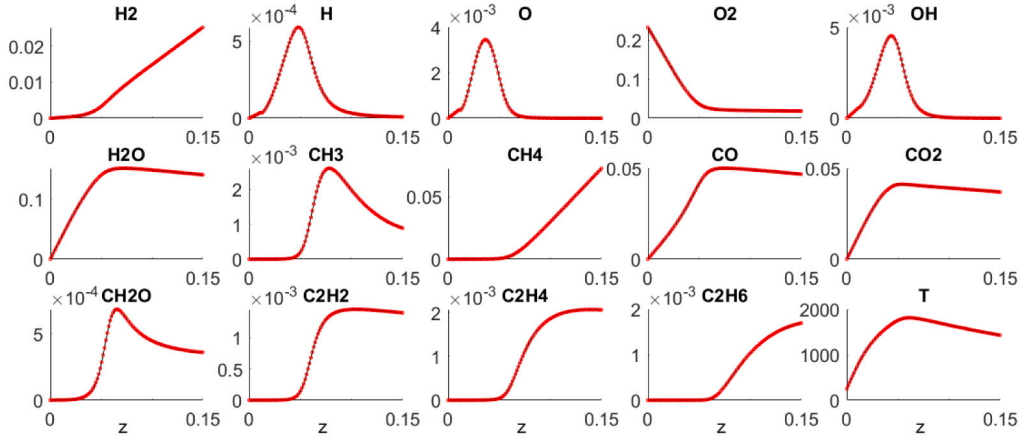

(c) Case 3.

Fig. 9. Species mass fractions and temperature profiles in the laminar CH_4/H_2 flamelet simulations. The DI results are plotted in black solid lines, while the ANN results are shown using red circle symbols. (For interpretation of the references to colour in this figure legend, the reader is referred to the web version of this article.)

uniform in the axial direction, with a cell size of 1 mm. In the radial direction, the cell size is about 0.6 mm in the central jet and bluff body region and then expands smoothly in the coflow region. The maximum CFL number is less than 0.2 using a time step of 10^{-6} s.

The mean and RMS values for several species mass fractions and temperature are collected at 5 axial locations: Z = 13, 30, 65, 90 and 120 mm. Fig. 14 shows the radial profiles of several major species mass fraction and temperature. It can be clearly seen that the ANN profiles are almost identical with DI profiles for both mean value and RMS value. The profiles of several minor species are shown in Fig. 15, where the ANN profiles and DI profiles nearly coincide in most plots. Some errors can be seen for CH_3 and CH_2O at low axial locations, where the ANNs overpredict the peak value. However, these errors are acceptable and the overall ANN profiles match the DI results very well.

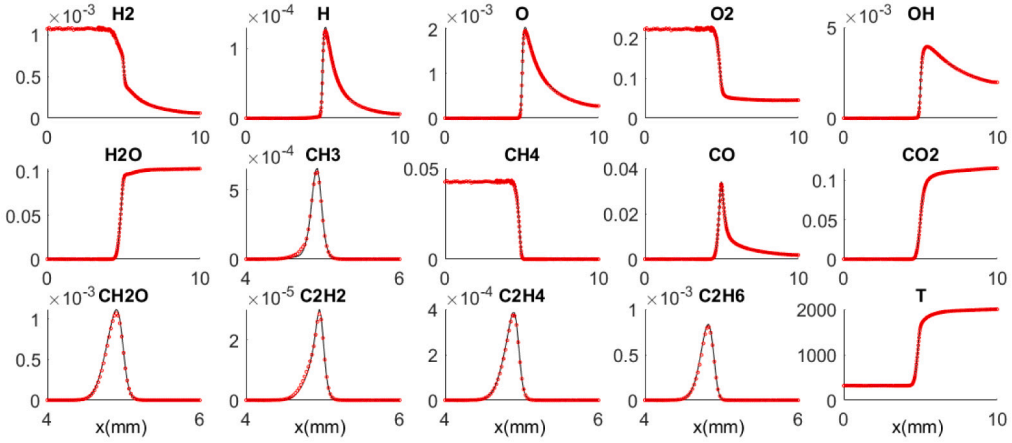

(a) Case A.

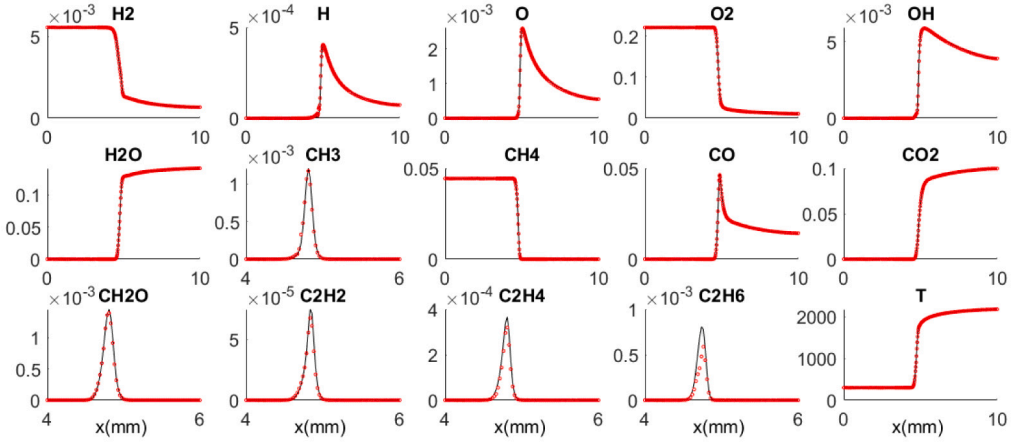

(b) Case B.

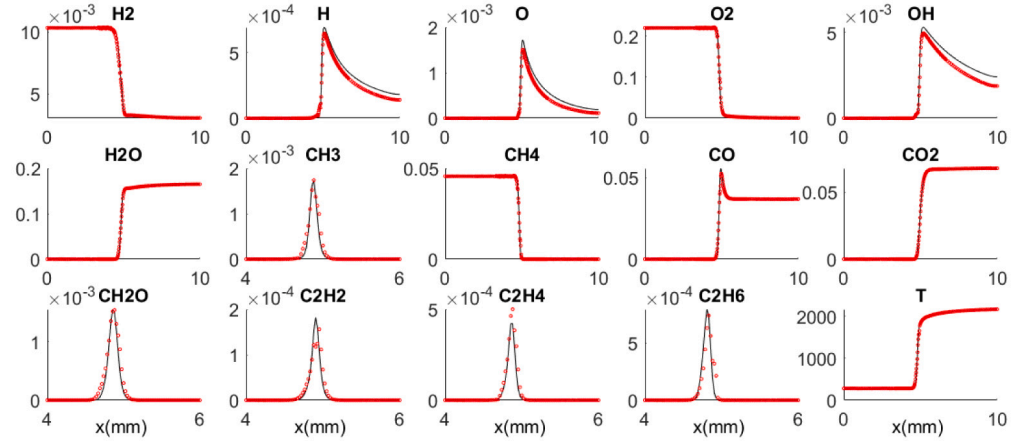

(c) Case C.

Fig. 10. Species mass fractions and temperature profiles in the 1-D laminar premixed CH_4/H_2 flame simulations. The DI results are plotted in black solid lines, while the ANN results are shown using red circle symbols. (For interpretation of the references to colour in this figure legend, the reader is referred to the web version of this article.)

Some discrepancies between the simulation results and experiment results are also evident in Fig. 14. Several factors will influence the simulation results of bluff body flames, including the grid resolution, the mechanism employed, the introduction of immersed boundaries [34] and so on. Since the present work aims at the ANN tabulation methodology, so the main focus is the generalisation and accuracy of the ANNs on chemistry tabulation. Although there are some differences between simulation results and experimental data, the agreement is overall reasonable and further improvement to match the experiment data is out of the scope of this work.

The mean temperature field and CH_4 mass fraction field of the cross section are plotted in Fig. 16. It can be seen that the flame structure is accurately produced by ANN simulation. The flame structure of HM1 is quite different from that of Sandia flames. One main feature of the flame structure is the large recirculation zone, which is induced by

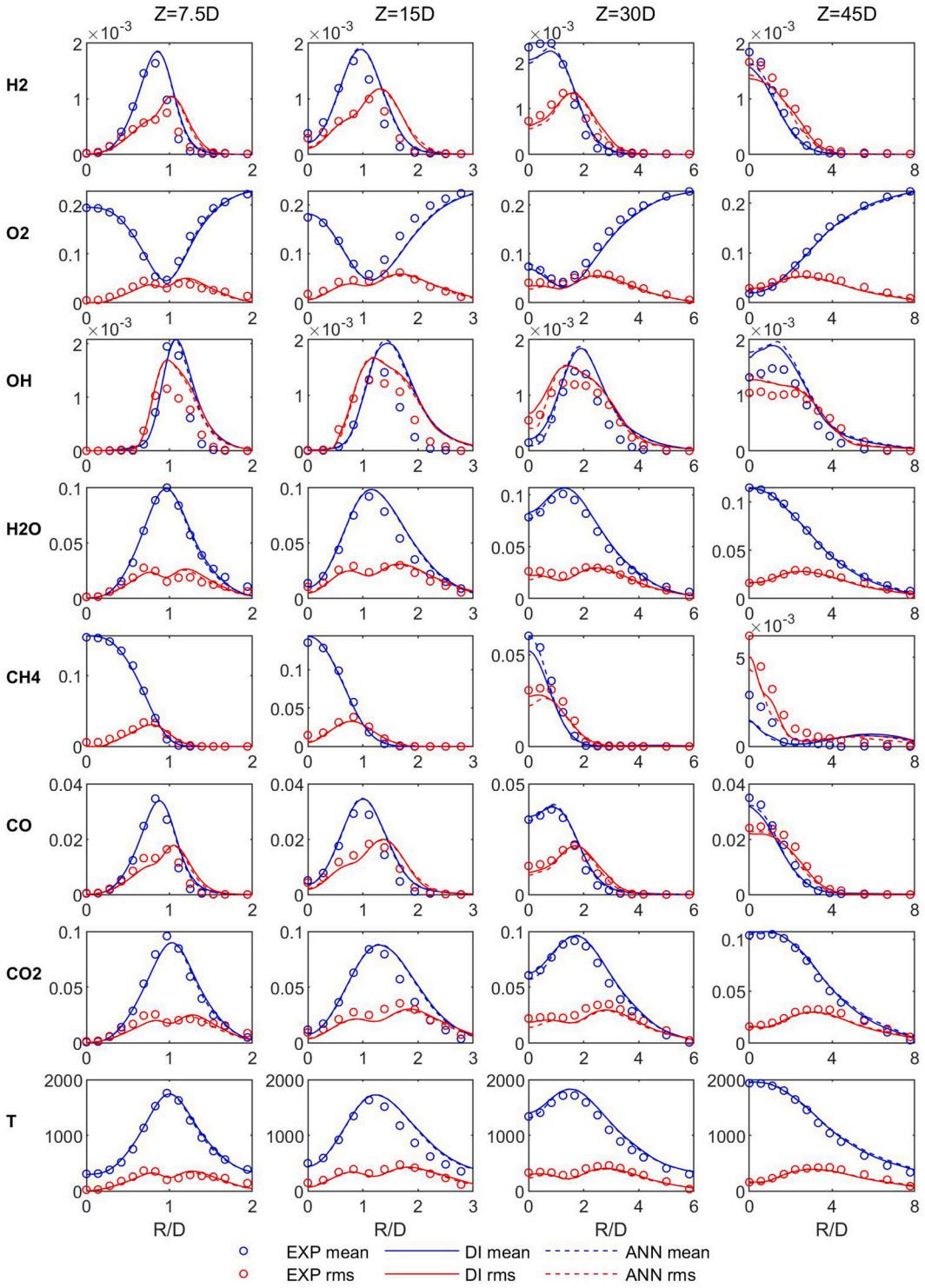

Fig. 11. Major species mass fractions and temperature of Sandia D. (For interpretation of the references to colour in this figure legend, the reader is referred to the web version of this article.)

the solid bluff body. This recirculation zone extends about one bluff-body diameter downstream of the face of the burner [33]. The peak temperature of this zone locates near the outer edge of the bluff-body, which can also be observed from the temperature radial profiles at location Z = 30 and 65 mm in Fig. 14. Downstream of the recirculation zone, the width of the flame becomes narrow and a neck zone is formed, where the temperature slightly decreases. Downstream of the neck zone, the rest of the flame shows a jet-like propagation. The mean temperature field in Fig. 16 clearly shows the location and distribution of these three regions, with very good agreement between ANN results and DI results.

Different from the Sandia flame simulation results, where the maximum errors are likely to occur at high axial locations, the ANN errors for the HM1 flame occur at low axial locations. This is mainly because of the accumulation of ANN errors. In the case of Sandia flame D, the data points at high axial locations go through more ANN reaction steps than those at low axial locations, so the ANN prediction error near the outlet is higher than those near the inlet. However, in the case of the

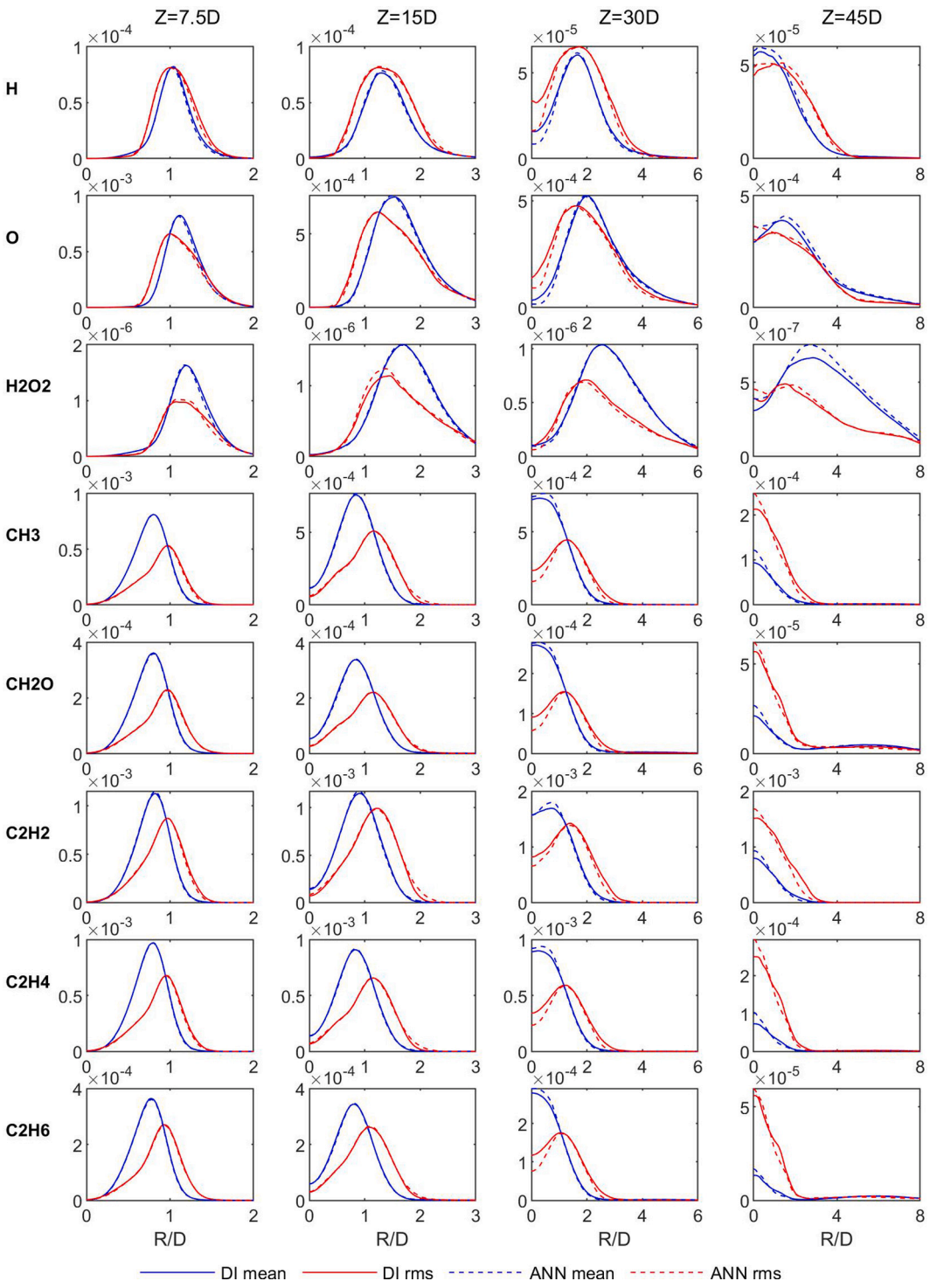

Fig. 12. Minor species mass fractions of Sandia D. (For interpretation of the references to colour in this figure legend, the reader is referred to the web version of this article.)

HM1 flame, a large recirculation zone occurs near the bluffy body, and the data points in this area will also go through many ANN reaction steps, resulting in greater accumulation of errors. Fig. 17 shows the 2-D streamlines of the mean velocity and the mean axial velocity field of both ANN and DI simulation results. Both streamline plots clearly show two large vortices, with one being close to the air side and another one close to the central fuel jet. The axial velocity in the recirculation zone is very low compared with the jet or coflow velocity. Data points in this area are likely to go through more time steps. Nevertheless, the accumulation of errors is still small and occurs mainly in minor species. For major species, the errors are negligible and the ANN predictions are accurate at all axial locations.

The CPU time comparison of the HM1 flame simulation is shown in Table 7. Compared with DI, the time taken by the reaction step is reduced by 93% using the ANNs, corresponding to a speed-up ratio of 13.7. The percentage of reaction time to total time is reduced from 84% to 27%, meaning that the computation of the chemical kinetics no longer poses a bottleneck.

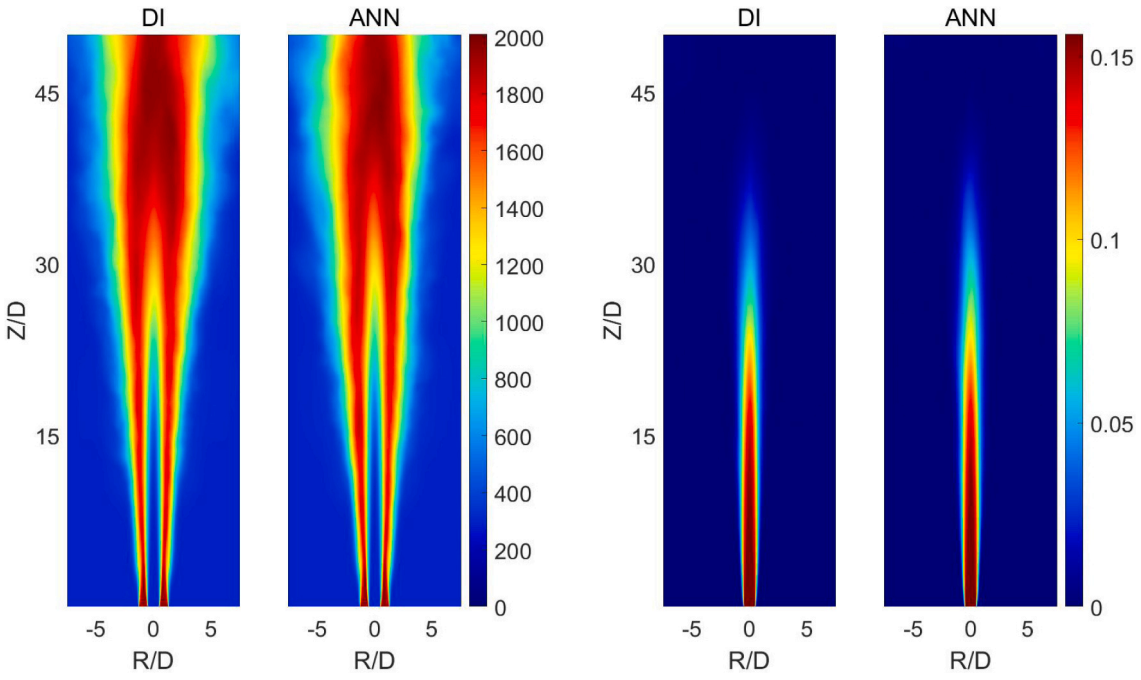

(a) Mean temperature (b) Mean CH_4 mass fraction

Fig. 13. Reactive scalar fields of Sandia flame D.

Table 7
Average CPU time for the HM1 flame simulation.

Method	Reaction time (t_R)	Total time (t_T)	t_R/t_T
DI	1	1.19	84%
ANN	0.073	0.27	27%

5. Conclusions

In the present work, the HFRD-MMLP thermochemistry tabulation method was extended to account for flames with fuel blends. The random data generation method endows the method with a generalisation capability, while the multiple MLPs improve the ANN predictive accuracy. An approach for generating random data so as to account for variable fuel ratio was developed and demonstrated on different laminar and turbulent flames. Furthermore, the applicability of the method to non-adiabatic problems was evaluated by simulating flames with radiative heat loss.

The ANNs were first tested on 1-D laminar premixed and diffusion flames. Methane flames and a series of methane/hydrogen flames with different fuel mixing ratios were employed and excellent agreement between ANN and DI results were obtained for all cases, indicating the applicability of the ANNs to both methane and methane/hydrogen flames. Subsequently, the ANNs were further evaluated in two turbulent flames: Sandia flame D and Sydney HM1 flame. These two flames have different fuel mixtures and flame structures. Sandia D flame is a piloted methane jet flame, while HM1 is a bluff body methane/hydrogen flame featuring a large recirculation zone. The ANN simulation results were in excellent agreement with those obtained via DI, and the flame structures were also captured with high accuracy. Radiation heat losses were considered, demonstrating the applicability of the method to non-adiabatic problems. Furthermore, a speed-up ratio of 13.7 (HM1)–17.4 (Sandia) in the reaction step as compared with DI was obtained.

The accurate simulations of 1-D laminar premixed flames indicate that the methodology can account for combustion simulations including differential diffusion. The introduction of direct differential diffusion into the transported PDF/stochastic field solution method [35] is relatively straightforward. However, the formulation of a *sgs* mixing model including differential diffusion effects remains problematic. If a suitable model can be devised then there is no reason to doubt that the ANN tabulation methodology presented here will be applicable.

The successful application of the augmented HFRD-MMLP methodology to different combustion problems including pure fuels, fuel blends and non-adiabatic problems indicates the generalisation capacity of the approach. Future work will be conducted in order to extend the methodology to more complex mechanisms and NO_x prediction.

Declaration of competing interest

The authors declare that they have no known competing financial interests or personal relationships that could have appeared to influence the work reported in this paper.

Acknowledgements

Tianjie Ding gratefully acknowledges the financial support provided by the China Scholarship Council (CSC) and the Department of Mechanical Engineering, Imperial College London, UK. For the computational resources, we are grateful to the Imperial College Research Computing Service (http://doi.org/10.14469/hpc/2232), the ARCHER UK National Supercomputing Service (http://www.archer.ac.uk) via the UK Consortium on Turbulent Reacting Flows (www.ukctrf.com) supported by EPSRC, UK grant EP/R029369/1 and the UK Materials and Molecular Modelling Hub partially funded by EPSRC, UK (EP/P020194/1 and EP/T022213/1).

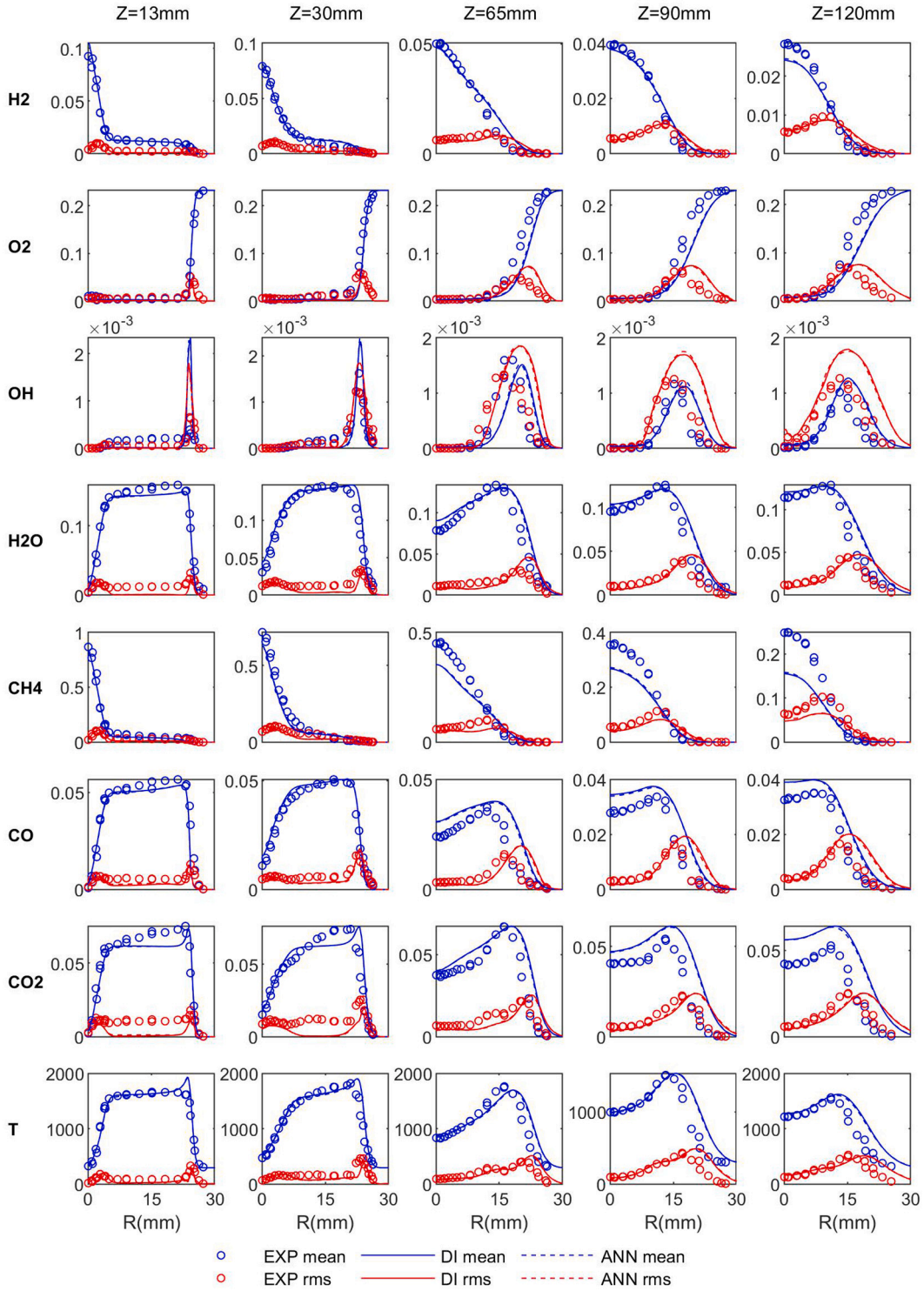

Fig. 14. Major species mass fractions and temperature of flame HM1. (For interpretation of the references to colour in this figure legend, the reader is referred to the web version of this article.)

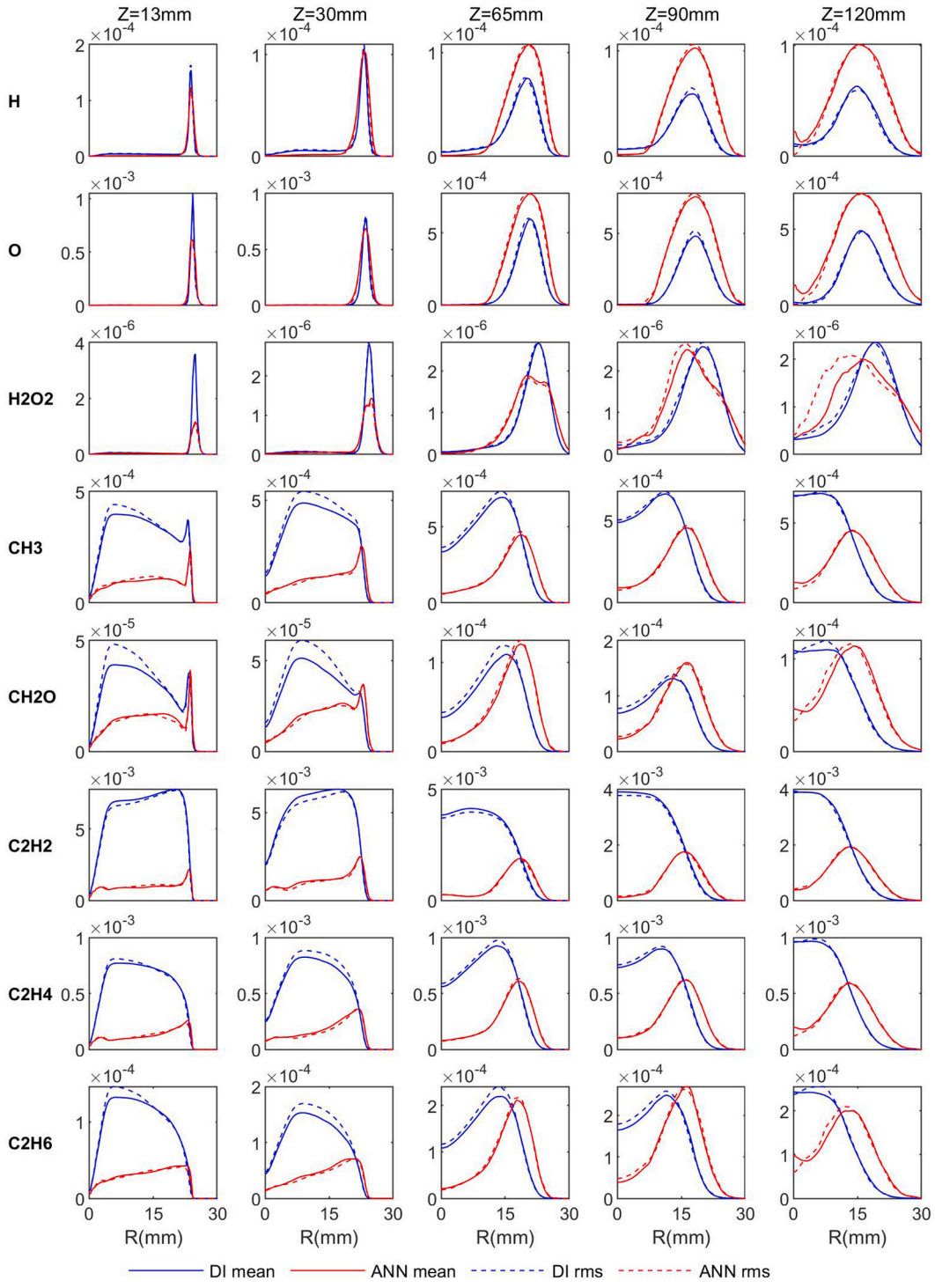

Fig. 15. Minor species mass fractions of flame HM1. (For interpretation of the references to colour in this figure legend, the reader is referred to the web version of this article.)

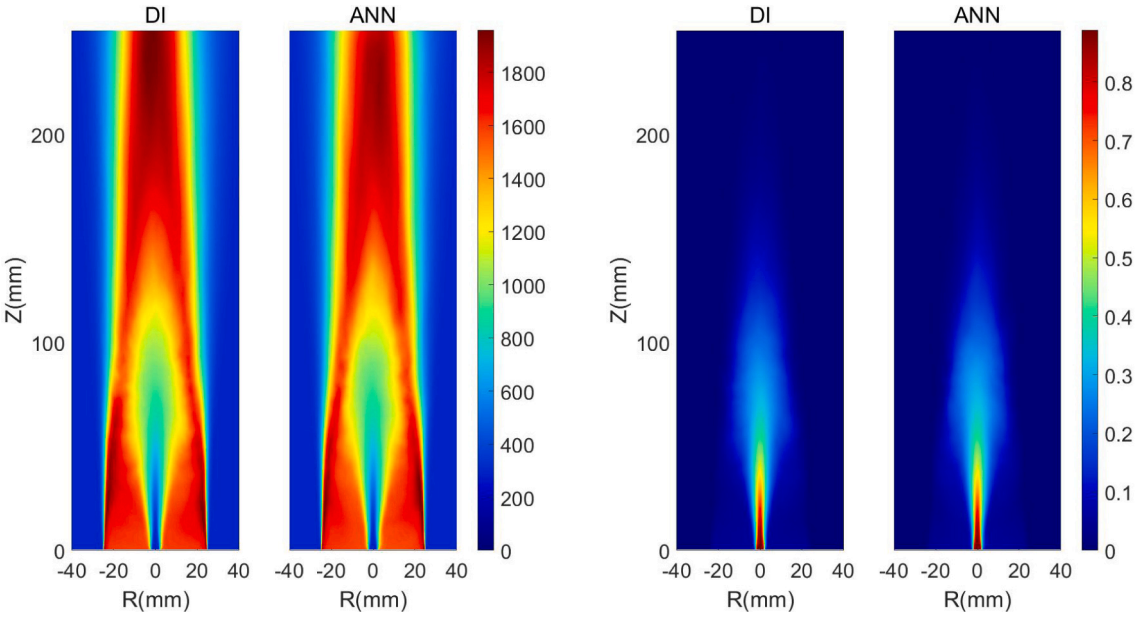

(a) Mean temperature (b) Mean CH_4 mass fraction

Fig. 16. Reactive scalar fields of flame HM1.

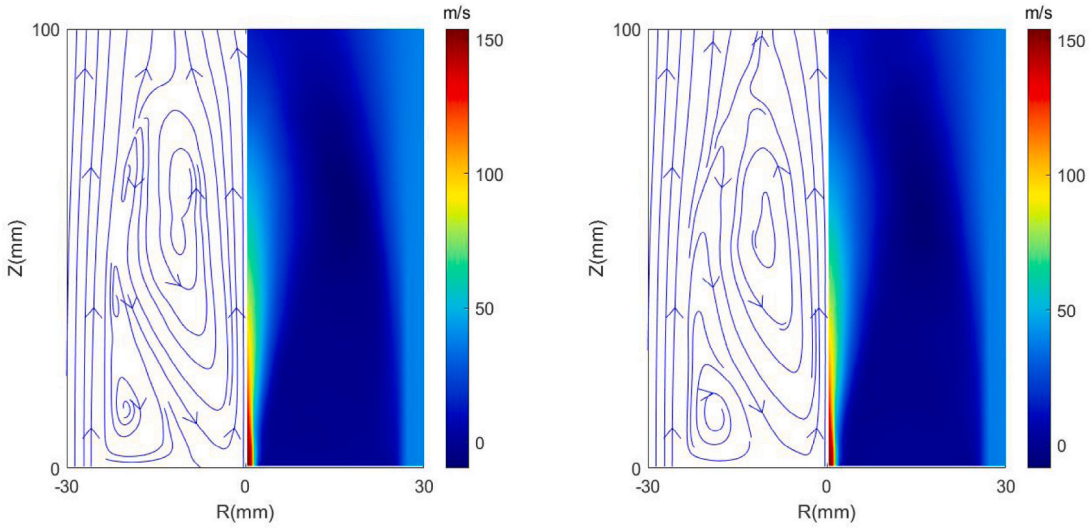

(a) DI (b) ANN

Fig. 17. Streamlines of 2-D mean velocity and mean axial velocity field.

References

[1] Ihme M, Chung WT, Mishra AA. Combustion machine learning: Principles, progress and prospects. Prog Energy Combust Sci 2022;91:101010.

[2] Christo FC, Masri AR, Nebot EM, Turanyi T. Utilizing artificial neural network and repro-modelling in turbulent combustion. In: IEEE international conference on neural networks - conference proceedings, Vol. 2. 1995, p. 911–6.

[3] Christo FC, Masri AR, Nebot EM. Artificial neural network implementation of chemistry with pdf simulation of H_2/CO_2 flames. Combust Flame 1996;106(4):406–27.

[4] Christo FC, Masri AR, Nebot EM, Pope SB. An integrated PDF/neural network approach for simulating turbulent reacting systems. Symp (Int) Combust 1996;26(1):43–8.

[5] Blasco JA, Fueyo N, Dopazo C, Ballester J. Modelling the temporal evolution of a reduced combustion chemical system with an artificial neural network. Combust Flame 1998;113(1–2):38–52.

[6] Blasco JA, Fueyo N, Larroya JC, Dopazo C, Chen Y-J. A single-step time-integrator of a methane-air chemical system using artificial neural networks. Comput Chem Eng 1999;23(9):1127–33.

[7] Blasco JA, Fueyo N, Dopazo C, Chen J-Y. A self-organizing-map approach to chemistry representation in combustion applications. Combust Theory Model 2000;4(1):61–76.

[8] Chatzopoulos AK, Rigopoulos S. A chemistry tabulation approach via rate-controlled constrained equilibrium (RCCE) and artificial neural networks (ANNs), with application to turbulent non-premixed $CH_4/H_2/N_2$ flames. Proc Combust Inst 2013;34(1):1465–73.

[9] Franke LLC, Chatzopoulos AK, Rigopoulos S. Tabulation of combustion chemistry via artificial neural networks (ANNs): Methodology and application to LES-PDF simulation of sydney flame l. Combust Flame 2017;185:245–60.

[10] An J, He G, Luo K, Qin F, Liu B. Artificial neural network based chemical mechanisms for computationally efficient modeling of hydrogen/carbon monoxide/kerosene combustion. Int J Hydrogen Energy 2020;45(53):29594–605.

[11] Kempf A, Flemming F, Janicka J. Investigation of lengthscales, scalar dissipation, and flame orientation in a piloted diffusion flame by LES. Proc Combust Inst 2005;30(1):557–65.
[12] Ihme M, Schmitt C, Pitsch H. Optimal artificial neural networks and tabulation methods for chemistry representation in LES of a bluff-body swirl-stabilized flame. Proc Combust Inst 2009;32 I(1):1527–35.
[13] Readshaw T, Ding T, Rigopoulos S, Jones WP. Modeling of turbulent flames with the large eddy simulation-probability density function (LES-PDF) approach, stochastic fields, and artificial neural networks. Phys Fluids 2021;33(3).
[14] Wan K, Barnaud C, Vervisch L, Domingo P. Chemistry reduction using machine learning trained from non-premixed micro-mixing modeling: Application to DNS of a syngas turbulent oxy-flame with side-wall effects. Combust Flame 2020;220:119–29.
[15] Hansinger M, Ge Y, Pfitzner M. Deep residual networks for flamelet/progress variable tabulation with application to a piloted flame with inhomogeneous inlet. Combust Sci Technol 2020;1–27.
[16] Ding T, Readshaw T, Rigopoulos S, Jones WP. Machine learning tabulation of thermochemistry in turbulent combustion: An approach based on hybrid flamelet/random data and multiple multilayer perceptrons. Combust Flame 2021;231.
[17] Sen BA, Menon S. Linear eddy mixing based tabulation and artificial neural networks for large eddy simulations of turbulent flames. Combust Flame 2010;157(1):62–74.
[18] Sen BA, Hawkes ER, Menon S. Large eddy simulation of extinction and reignition with artificial neural networks based chemical kinetics. Combust Flame 2010;157(3):566–78.
[19] Karim GA, Wierzba I, Al-Alousi Y. Methane-hydrogen mixtures as fuels. Int J Hydrogen Energy 1996;21(7):625–31.
[20] Ma F, Wang Y, Liu H, Li Y, Wang J, Ding S. Effects of hydrogen addition on cycle-by-cycle variations in a lean burn natural gas spark-ignition engine. Int J Hydrogen Energy 2008;33(2):823–31.
[21] Frenklach M, Wang H, Goldenberg M, Smith GP, Golden DM, Bowman C, Hanson R, Gardiner W, Lissianski V. GRI-mech - an optimized detailed chemical reaction mechanism for methane combustion. Tech. rep., Gas Research Institute Topical Report No. GRI-95/0058, 1995.
[22] Peters N. Turbulent combustion. Cambridge University Press; 2000.
[23] Brown PB, Byrne GD, Hindmarsh AC. VODE: A variable-coefficient ODE solver. SIAM J Sci Statist Comput 1989;10(5):1038–51.
[24] International workshop on measurement and computation of turbulent flames. URL https://tnfworkshop.org/.
[25] Jones WP, Prasad VN. Large eddy simulation of the sandia flame series (D-F) using the Eulerian stochastic field method. Combust Flame 2010;157(9):1621–36.
[26] Piomelli U, Liu J. Large-eddy simulation of rotating channel flows using a localized dynamic model. Phys Fluids 1995;7(4):839–48.
[27] Jones WP, di Mare F, Marquis AJ. LES-BOFFIN: user's guide. 2002.
[28] Prasad VN. Large eddy simulation of partially premixed turbulent combustion (Ph.D. thesis), Imperial College London (University of London); 2011.
[29] Grosshandler WL. RADCAL: a narrow-band model for radiation, calculations in a combustion environment. NIST technical note 1402, 1993.
[30] Barlow RS, Karpetis AN, Frank JH, Chen J-Y. Scalar profiles and NO formation in laminar opposed-flow partially premixed methane/air flames. Combust Flame 2001;127(3):2102–18.
[31] Barlow RS, Frank JH. Effects of turbulence on species mass fractions in methane/air jet flames. Symp (Int) Combust 1998;27(1):1087–95.
[32] Schneider C, Dreizler A, Janicka J, Hassel EP. Flow field measurements of stable and locally extinguishing hydrocarbon-fuelled jet flames. Combust Flame 2003;135(1–2):185–90.
[33] Dally BB, Masri AR, Barlow RS, Fiechtner GJ. Instantaneous and mean compositional structure of bluff-body stabilized nonpremixed flames. Combust Flame 1998;114(1–2):119–48.
[34] Kempf A, Lindstedt RP, Janicka J. Large-eddy simulation of a bluff-body stabilized nonpremixed flame. Combust Flame 2006;144(1–2):170–89.
[35] Jones WP, Marquis AJ, Vogiatsaki K. Assessing the effect of differential diffusion for stratified lean premixed turbulent flames with the use of LES-PDF framework. 2019;191:1003–1018.